$3CaH_2+4MgB_2+CaF_2$ Reactive Hydride Composite as a Potential Hydrogen Storage Material: Hydrogenation and dehydrogenation pathway

K. Suarez-Alcantara[1], J. M. Ramallo-Lopez[2], U. Boesenberg[1], I. Saldan[1], C. Pistidda[1], F. G. Requejo[2], T. Jensen[3], Y. Cerenius[4], M. Sørby[5], J. Avila[6], J. Bellosta von Colbe[1], K. Taube[1], Thomas Klassen[1], M. Dornheim[1].

[1] Institute of Materials Research, Materials Technology, Helmholtz-Zentrum Geesthacht, D-21502 Geesthacht Germany.

[2] Instituto de Investigaciones Fisicoquímicas, Teóricas y Aplicadas (INIFTA), Universidad Nacional de La Plata - CONICET, Suc. 4 C. C. 16 (1900) La Plata, Argentina.

[3] Aarhus University, Interdiciplinary Nanoscience Center, Department of Chemistry. Langelandsgade 140, Aarhus C, DK-8000, Denmark.

[4] Synchrotron MaxLab. Lund University MAX-lab Ole Römers väg 1 SE-223 63 Lund Sweden.

[5] IFE Institute for Energy Technology Instituttveien 18 NO-2007 Kjeller, Norway.

[6] Synchrotron SOLEIL. L'Orme des Merisiers Saint-Aubin - BP 48 91192 GIF-sur-YVETTE CEDEX

Abstract

A Reactive Hydride Composite (RHC) with initial composition $3CaH_2+4MgB_2+CaF_2$ was studied by in situ synchrotron radiation powder X-ray diffraction (SR-PXD) and X-ray Absorption Near Edge Structure (XANES) at the B K-edge and at the Ca K-edge. The hydrogenation reaction proceeds by an unknown intermediate. No evidence of intermediates was observed during the dehydrogenation reaction. B and Ca K-edges XANES results hint to a closed interaction CaF_2 and $Ca(BH_4)_2$. The main function of CaF_2 in the $3CaH_2+4MgB_2+CaF_2$ RHC is as a dopant for the hydrogenation and dehydrogenation reactions.

Key words: Hydrogen storage, metal hydrides, borohydrides, Reactive Hydride Composite, fluorine substitution, in-situ synchrotron radiation.

1. Introduction

Hydrogen storage in light metal hydrides is considered as a possible solution for future fuel cell applications. At present, no single metal hydride fulfills all requirements on capacity, reaction kinetics and reaction enthalpy necessary for practical applications. A step forward in the

development of new materials for hydrogen storage are the so called "Reactive Hydride Composites (RHC)" [1, 2] or "destabilized hydrides" [3, 4, 5]. In this approach, two hydrides react to form a new compound. This formation is exothermic and thus the overall reaction enthalpy is lowered, allowing for high hydrogen capacities and low reaction temperatures. The work on destabilized systems was initially performed by Reilly *et at* in the system $2Mg_2Cu + 3H_2 \leftrightarrow 3MgH_2 + MgCu_2$ [6]. Nowadays the most prominent and studied system is the $2LiBH_4+MgH_2 \leftrightarrow 2LiH+MgB_2+4H_2$ RHC [7, 8, 9, 10]. Other interesting systems are, e.g. $2NaBH_4+MgH_2 \leftrightarrow 2NaH+MgB_2+4H_2$ [11, 12, 13, 14] and $Ca(BH_4)_2+MgH_2 \leftrightarrow CaH_2+MgB_2+4H_2$ [15] composites. In contrast to the pure borohydrides, the RHC show good reversibility under much more moderate conditions [1]. However, strong kinetic constraints hinder the possible practical applications [2]. To achieve a solution of the hydrogen storage problem it is necessary both, to improve kinetics and to tune the thermodynamics of the respective hydrogenation/dehydrogenation reactions. Wang *et al* reported that Fluorine can enhance the surface reactivity of rare earth-nickel based hydrides [16]. The dehydrogenation thermodynamics can be altered in complex hydrides by the so-called functional anion concept as shown in $NaAlH_4$ [17, 18]. The addition of fluorine in the CaH_2/ MgB_2 system had demonstrated a favorable effect for hydrogen storage purposes, increasing the hydrogen uptake from 3.5 wt% to 7.0 wt% at 130 bar hydrogen pressure and 350°C at the same reaction time [19]. The fluorine doped composite $3CaH_2+4MgB_2+CaF_2$ was selected to perform in-situ synchrotron radiation powder X-ray diffraction (SR-PXD) and X-ray Absorption Near Edge Structure (XANES) at the B K-edge and at the Ca K-edge. The $3CaH_2+4MgB_2+CaF_2$ composite has a 7.7 wt% theoretical hydrogen storage capacity by the formation of $Ca(BH_2)_4$ and MgH_2 after hydrogenation. The measured hydrogen capacity storage was about 7 wt% and the system presents good hydrogenation kinetics [19]. However, the details of the reaction pathway are unsolved so far. In-situ SR-PXD experiments are suitable to investigate the reaction pathway and structural features of RHC for hydrogen storage. XANES is sensitive to the local bonding configuration of each type of atom [20]. This selective technique is useful to determine the local structure of the composites and revealed the role of the CaF_2.

2. Experimental details

The $3CaH_2+4MgB_2+CaF_2$ composite was prepared by two stages of ball milling as described elsewhere [19]. The first stage was the milling of CaH_2 and CaF_2, as a second step CaF_2-CaH_2 mixture and MgB_2 were milled together in a SPEX mill. The composite was exposed to two cycles of hydrogenation and dehydrogenation at 350 °C. The hydrogenation pressure was 130 bar H_2 and the dehydrogenation pressure was set to 0.1 bar H_2. The hydrogenation and

dehydrogenation experiments lasted 12 hours each in a PCTPro-2000 (SETARAM Instrumentation) as described elsewhere [19]. Briefly, the hydrogenation and dehydrogenation reactions were made in a repetitive and cumulative way. A sample of the as milled powder was hydrogenated and then the experiment was stopped. A second sample was hydrogenated and dehydrogenated, and then the experiment was stopped. A third sample was first hydrogenated, dehydrogenated and re-hydrogenated. A fourth sample was exposed to two cycles of hydrogenation / dehydrogenation.

The structural feature in the first hydrogenation/ dehydrogenation cycle was investigated by in situ time-resolved SR-PXD (beamline I711, MAX II synchrotron at MaxLab) [21]. It operates at λ = 0.939 Å X -ray wavelength and with a MAR165 CCD detector. In the hydrogenation setup, the as milled sample was heated at 5 °C min^{-1} from room temperature to 350 °C and then kept isothermal for 4 hours under 130 bar of hydrogen pressure. For the respective dehydrogenation reaction, a previously hydrogenated sample was heated at 5 °C min^{-1} from room temperature to 350 °C and kept isothermal for 1 hour at 0.1 bar H_2. The second dehydrogenation reaction was studied by in situ time resolved SR-PXD at the Swiss Norwegian beamline (MB01A) at the European Synchrotron Radiation Facility, λ = 0.7 Å X -ray wavelength and an imaging plate system (MAR345). A sample exposed to one cycle of hydrogenation/ dehydrogenation and then re-hydrogenated was heated at 5 °C min^{-1} from room temperature to 350°C and kept isothermal for 30 minutes at 0.1 bar H_2.

XANES experiments at the B K-edge were performed at the Antares beamline of the Soleil synchrotron in Paris, France. Powders were mounted on a Cu tape. The samples were transferred from a glove box to the Ultra-High-Vacuum chamber of the beamline without air exposure. The measurements were made in Total Electron Yield mode. XANES experiments at the Ca K-edge were performed at the A1 beamline of the DESY synchrotron, Hamburg, Germany, and at the XAFS2 beamline of the Laboratorio Nacional de Luz Sincrotron (LNLS), Campinas, Brazil in transmission mode. Samples were pressed in pellets and sealed with Kapton foil in a dedicated sample holder. Un-milled $Ca(BH_4)_2$, $Ca(BF_4)_2$, MgB_2, CaF_2 and CaH_2 or their mixtures produced by ball milling (SPEX mill, 5 hours milling time, 10:1 ball to powder ratio) were used as references.

3. Results and discussion

Figure 1 presents the in situ SR-PXD results of the first hydrogenation of the $3CaH_2+4MgB_2+CaF_2$ composite. The patterns are shown in a white (near zero intensity) to blue (high intensity) scale map. For purposes of comparison, all patterns were plotted in q-space [$Å^{-1}$]

instead of 2θ degree; with $q = 4\pi \sin(\theta/\lambda)$, where θ is half the scattering angle, and λ is the wavelength. The peaks observed at room temperature correspond to the raw materials CaF_2, CaH_2 and MgB_2 besides Fe as a contamination from the milling vial.

The first change observed with heating is the increase of peak intensity due to recrystallization or coarsening of the micro/nano-particles produced by the ball milling process. The recrystallization is particularly evident for CaF_2. The evolution of two unidentified peaks at 1.56 Å $^{-1}$ and 2.55 Å $^{-1}$ was observed at 270°C. As the temperature increased these peaks shifted to higher q [Å $^{-1}$] values and two changes in intensity were observed in those peaks (graphical abstract and Figure 1). The first of them was an increase in peak intensity as the temperature reaches 350°C and then a decrease in peak intensity until they disappeared completely after 1 hour in isothermal (350°C) condition. Apparently these peaks are due to intermediates, however none of the proposed intermediates or phase changes for the hydrogenation/ dehydrogenation reactions in the $Ca(BH4)_2$ + MgB_2 composite [15] or $Ca(BH_4)_2$ [22, 23, 24, 25, 26, 27] fit them. In a recent study by in situ SR-PXD of the hydrogenation of CaH_2+MgB_2 mixture at 350°C and 120 bar, no indication of intermediaries was observed [28]. This suggests a change in the reaction pathway by the addition of CaF_2 compared with the undoped RHC. The formation of the β-$Ca(BH_4)_2$ phase started at 280°C as indicated by the peak at 1.27 Å $^{-1}$ (graphical abstract and Figure 1) and it is followed by the formation of MgH_2. During cooling, due to the β to α-$Ca(BH_4)_2$ phase transition the peaks of the β-$Ca(BH_4)_2$ phase almost completely disappear. The peak at 1.69 Å $^{-1}$ remains unchanged.

First dehydrogenation reaction is presented in Figure 2. The α-$Ca(BH_4)_2$/β-$Ca(BH_4)_2$ mixture, MgH_2, unreacted CaF_2 and an unidentified peak at 1.60 Å $^{-1}$ were observed at room temperature. At 140°C, while the heating of the hydrogenated sample continues, the α to β-$Ca(BH_4)_2$ phase transition was observed to take place. At 275°C, changes in the peak intensity of the $Ca(BH_4)_2$ phase occur indicating the beginning of the dehydrogenation reaction. The $Ca(BH_4)_2$ peaks vanish before reaching 350° C while the unidentified peak at 1.60 Å $^{-1}$ vanishes after 15 minutes at isothermal condition (350°C). Finally, peaks corresponding to CaH_2, MgB_2, CaF_2, and Mg were observed. During the dehydrogenation reaction, no intermediates were observed by PXD. In addition, previously performed DSC measurements did not reveal any evidence of other phase transformations like melting [19]. Based on these data, the dehydrogenation reaction so far has to be considered as a one-step reaction.

The second dehydrogenation reaction mapping is presented in Figure 3. Two characteristics are different regarding the first dehydrogenation: 1) the absence of the unknown peak at 1.60 Å $^{-1}$ and 2) a shift to lower desorption temperature. The dehydrogenation reaction is completed at around 320°C. This observation agrees well with DSC results[19] of the first, second and third

dehydrogenation processes where such a lowering of dehydrogenation temperature with cycling was observed as well. Both characteristics suggest a change in the dehydrogenation pathway. However, the dehydrogenation at 350°C and 0.1 bar produces the formation of Mg instead of MgB_2 and an unknown compound. This effect can reduce the reversibility (re-hydrogenation) of the system. The formation of MgB_2 instead of Mg could be favored by a low-pressure dehydrogenation, as was concluded in a recent study on $LiBH_4/MgH_2$ reactive hydride composite [7, 8]. The 0.1 bar for dehydrogenation was selected in order to complete the dehydrogenation under the time scale of a synchrotron experiment. A detailed study at higher dehydrogenation pressures must be completed. It is also necessary to improve kinetics and reduce operational temperatures [29]. Further work is going in that direction.

Up to this point, the possibility of hydrogen storage in the $3CaH_2+4MgB_2+CaF_2$ composite was shown, however the role of fluorine remains ambiguous. Several studies present the effect of CaF_2 on dehydrogenation of $Ca(BH_4)_2$. As discussed elsewhere [19], Kim *et al* [30] claim the formation of a solid solution of $CaF_{2-x}H_x$ in CaF_2 after doping and cycling $Ca(BH_4)_2$ with TiF_3 or NbF_5. Kim *et al* [30] and Rongeat *et al* [29] claim a possible enhanced reversibility originated by the formation of $CaF_{2-x}H_x$ phases. Lee *et al* suggest that CaF_2 act as seed for the growing of CaH_2 during dehydrogenation of $Ca(BH4)_2+CaF_2$ [31]. Lee also proposes that the calcium halide directs the dehydrogenation of $Ca(BH4)_2+CaF_2$ through the formation of CaH_2 and CaB_6 without forming reaction intermediates or side products such as CaB_2H_x. The solid solution CaF_2-CaH_2 plays an important role during dehydrogenation [31, 32]. However, since $CaF_{2-x}H_x$ and CaF_2 have the same crystal structure (space group no. 225) and very similar lattice parameters (a = 5.4712 Å for CaF_2 and a = 5.4520 Å for $CaF_{2-x}H_x$, x=1.24) [32] to observe the solid solution CaF_2-CaH_2 by in-situ SR-XPD is difficult and no evidence of the solid solution was observed in the present work.

To help clarifying whether the hydrogenation of CaH_2/ MgB_2 in presence of CaF_2 leads to Fluorine substituted products or just a closed interaction among the products and the CaF_2, XANES experiments were carried out. XANES is a more suitable technique than in-situ SR-PXD for the determination of changes in the neighborhood of the absorbing atom.

Studies at the B K-edge have been performed e.g. in B-containing glasses [33] and Boron nitride [34] structures. In the present work, the local structure variations around the B atom in RHC were investigated by XANES at the B K-edge. To our knowledge this is the first time that B K-edge in $Ca(BH_4)_2$ and related compounds was investigated. The $Ca(BH_4)_2$ spectrum (Figure 4) consists mainly of the white line at 193.2 eV, and a very broad peak above 195eV. The white line at 193.2 eV is similar to a peak around 191 eV attributed by Jimenez *et al* [34, 35] to a B atom surrounded by four N in boron nitride structures. In that study [34, 35] the 191 eV peak was not as intense as in the

present spectra in Fig. 4. According to boron nitride and boron carbide [34, 35] NEXAFS studies, the intense peak around 192 eV– 194 eV is attributed to the transition of B 1s electrons to the unoccupied B $2P_z$ (π^* resonance). The broad peak extending beyond 195eV is attributed to transitions of B 1s electrons to unoccupied σ^* states [34, 35]. These observations are consistent with the structure of $Ca(BH_4)_2$ in which the B atom is surrounded by four H atoms in a tetragonal structure. Figure 4 also include the XANES Boron K-edge of $Ca(BF_4)_2$, MgB_2 and the composites $Ca(BH_4)_2$+MgH_2 and $Ca(BH_4)_2$+CaF_2. The B K-edge spectra of $Ca(BF_4)_2$ present intense white line at 192.6 and a broad peak above 195eV. The general shape of the Boron K-edge spectra of $Ca(BF_4)_2$ present similitudes with the $Ca(BH_4)_2$ spectra; however in the $Ca(BF_4)_2$ spectra the white line is shifted to lower energy and the intensity of the pre-edge peak is bigger. The characteristic of the broad peak above 190 eV in the $Ca(BF_4)_2$ spectra is completely different to the $Ca(BH_4)_2$ spectra. The $Ca(BF_4)_2$ spectra was taken in the un-milled material due to this material decompose when ball milled. The $Ca(BH_4)_2$ and MgB_2 materials are enough stable during milling process but to be comparable with $Ca(BF_4)_2$ they were taken as un-milled. The MgB_2 present an intense with line at 192.2 eV. The intense milling (in SPEX mill) of $Ca(BH_4)_2$+MgH_2 and $Ca(BH_4)_2$+CaF_2 introduce changes in the white line position and relative intensity concerning the $Ca(BH_4)_2$. The B K-edge spectrum of $3CaH_2$+$4MgB_2$+CaF_2 after cycling is presented in Figure 5. They consist of a pre-edge peak at 191.5 eV, the white line at 193 eV and a broad peak above 195 eV. The XANES spectrum of $3CaH_2$+$4MgB_2$+CaF_2 after cycling remains closer that the $Ca(BH_4)_2$+CaF_2 with subtle changes in the base line according the hydrogenated or dehydrogenated state. Handa *et al* [36] measured XAS spectra of lithium halides and obtained a relationship between white line position and the electronegativity difference of the Li-halide bond. In event of Fluorine substitution, a similar shift of the B K-edge white line could be expected as the B-H or B-F could take place. However, not significant changes in the composites were observed. Moreover, the characteristics of the pre-edge peak and the broad peak above 190 eV indicate that not Fluorine-substitution takes place and outline the role of CaF_2 as a dopant for the CaH_2/ MgB_2 reactive hydride composite.

Figure 6 shows the XANES spectra at the Ca K-edge of (un-milled) CaF_2, CaH_2, $Ca(BH_4)_2$, $Ca(BF_4)_2$, and $3CaH_2$+$4MgB_2$+CaF_2 after the 1st hydrogenation. The XANES spectra show characteristic features that can be used as finger print of each phase [37]. The spectra of $3CaH_2$+$4MgB_2$+CaF_2 after the 1st hydrogenation and $Ca(BH_4)_2$ present the same general shape. The main difference between the $Ca(BH_4)_2$ spectrum and those of the other species is observed at the pre-edge peak around 4040 eV and at the absorption edge, which is not present in the $Ca(BH_4)_2$. The pre-edge peak observed at ca. 4040 eV corresponds to a forbidden 1s→3d

transition, only allowed in non-centrosymmetric sites [38]. Peaks at ca. 4060 and 4080 eV were observed in the spectrum of $Ca(BF_4)_2$ and CaF_2 which are not present in $Ca(BH_4)_2$. These features are also present in the spectrum of $3CaH_2+4MgB_2+CaF_2$ after the 1st hydrogenation. Its XANES spectrum can be described mainly as a linear combination of $Ca(BH_4)_2$ and CaF_2.

Figure 7 shows the Fourier transforms of the XANES oscillations at the Ca K-edge of $3CaH_2+4MgB_2+CaF_2$ samples and further Ca-containing compounds. Both CaF_2 and CaH_2 present peaks at the same distances but the amplitude of CaF_2 peaks is bigger, what is a consequence of the fact that the heavier fluorine atoms produce more pronounced oscillations in the XANES signal than hydrogen atoms. The Fourier transform after the first hydrogen absorption cycle presents the same peak positions than that of $Ca(BH_4)_2$, but the amplitudes of the peaks are bigger. This suggests the presence of fluorine atoms in the first coordination shells of Ca, but not in a CaF_2 structure, as the Ca-Ca peak at 3.3 Å is not present. However, $Ca(BF_4)_2$ was not formed according to XANES results at the B K-edge, so a different compound should be present. After the desorption process, the Fourier Transform of the XANES signal resembles that of the CaH_2, including the appearance of the Ca-Ca coordination shell at 3.3 Å, however the peak amplitude is smaller. Thus, CaH_2, CaF_2 or even a $CaH_{2-x}F_x$ solid solution could be present. After the second absorption cycle, the peak at 3.3 Å remains almost unaltered indicating that this cycle is proceeding through a different pathway than the first one.

4. Conclusions

The hydrogenation and dehydrogenation reactions of the composite $3CaH_2+4MgB_2+CaF_2$ were investigated by in-situ SR-PXD. The hydrogenation reaction proceeds by an unknown intermediary. For the dehydrogenation reaction there is no clear evidence of an intermediary, a concerted reaction pathway is proposed. The first and second dehydrogenation pathways are different regarding the reduction of dehydrogenation temperature as cycling proceeds and the presence of unknown compounds formed at the hydrogenation stages. B and Ca K-edge XANES results together with the in situ SR-PXD suggest that only a minor part of CaF_2 interacts directly with B after hydrogenation. Ca K-edge results suggest that a small proportion of $CaH_{2-x}F_x$ solid solution could be present. Therefore, the results are still consistent with kinetics studies[19] claiming that the main function of CaF_2 in the CaH_2+MgB_2 RHC is as a dopant affecting the hydrogenation and dehydrogenation pathway and producing unknown products.

5. Acknowledgments

The research leading to these results has received funding from the European Community's Seventh Framework Programme FP7/2007-2013 under grant agreement No 226943- FLYHY.
The authors appreciate the facilities and technical support at Antares Beamline of the SOLEIL Synchrotron especially the support by Dr. M. C. Asensio. The authors appreciate the facilities and technical support at I711 beamline at MaxLab Synchrotron. The authors appreciate the facilities and technical support at the Swiss Norwegian beamline (MB01A) at the European Synchrotron Radiation Facility. The authors appreciate the facilities and technical support at A1 beamline at DESY synchrotron facility. The authors appreciate the facilities and technical support at the XAFS2 beamline of the Laboratorio Nacional de Luz Sincrotron (LNLS), Campinas, Brazil. This work was partly supported by LNLS under proposal D04B-XAFS1-9865. K. Suarez-Alcantara appreciates the valuable comments on XAS techniques of Dr. Sophie Canton, MaxLab Synchrotron.

6. References

(1) Barkhordarian, G.; Klassen, T.; Dornheim, M.; Bormann, R. J. Alloys and Compounds **2007**, 440, L18-L21.

(2) Dornheim, M.; Doppiu, S.; Barkhordarian, G.; Boesenberg, U.; Klassen, T.; Gutfleisch, O.; Bormann, R. Scripta Materialia **2007**, 56, 841-846.

(3) Vajo, J. J.; Skeith, S. L.; Mertens, F. J. Phys. Chem. B **2005**, 109, 3719-3722.

(4) Vajo, J. J.; Salguero, T. T.; Gross, A. F.; Skeith, S.L.; Olson G. L. J. Alloys and Compounds **2007**, 446-447, 409-414.

(5) Alapati, S. V.; Johnson, J. K.; Sholl D. S. J. Phys. Chem. B **2006,** 110, 8769-8776

(6) Reilly, J. J.; Wiswall, R. H. Inorg. Chem. **1967**, 6, 2220-2223.

(7) Bösenberg, U.; Ravnsbaek, D.B.; Hagemann, H.; D'Anna, V.; Minella, C.B.; Pistidda, C.; van Beek, W.; Jensen, T.R.; Bormann, R.; Dornheim, M. J. Phys. Chem. C **2010**, 114, 15212-15217.

(8) Bösenberg, U.; Kim, J.W.; Gosslar, D.; Eigen, N.; Jensen, T.R.; Bellosta von Colbe, J.M.; Zhou, Y.; Dahms, M.; Kim, D.H.; Günther, R.; Cho, Y.W.; Oh, K.H.; Klassen, T.; Bormann, R.; Dornheim, M. Acta Materialia **2010,** 58, 3381-3389.

(9) Bösenberg, U.; Vainio, U.; Pranzas, P.K.; Bellosta Von Colbe, J.M.; Goerigk, G.; Welter, E.; Dornheim, M.; Schreyer, A.; Bormann, R. Nanotechnology **2009**, 20, 204003-9.

(10) Vajo, J. J.; Olson, G. L. Scripta Materialia **2007**, 56, 829–834.

(11) Garroni, S.; Milanese, C.; Girella, A.; Marini, A.; Mulas, G.; Menéndez, E.; Pistidda, C.; Dornheim, M.; Suriñach, S.; Baró, M.D. International Journal of Hydrogen Energy **2010**, 35, 5434-5441.

(12) Nwakwuo, C.; Pistidda, C.; Dornheim, M.; Hutchison, J.L.; Sykes, J.M. Scripta Materialia **2011**, 64, 351-354.

(13) Pistidda, C.; Garroni, S.; Minella, C.B.; Dolci, F.; Jensen T.R.; Nolis, P.; Bösenberg, U.; Cerenius, Y.; Lohstroh, W.; Fichtner, M.; Baró, M.D.; Bormann, R.; Dornheim, M. Journal of Physical Chemistry C **2010**, 114, 21816-21823.

(14) Pistidda, C.; Barkhordarian, G.; Rzeszutek, A.; Garroni, S.; Minella, C.B.; Baró, M.D.; Nolis, P.; Bormann, R.; Klassen, T.; Dornheim, M. Scripta Materialia **2011**, 64, 1035-1038.

(15) Barkhordarian, G.; Jensen, T.R.; Doppiu, S.; Boesenberg, U.; Borgschulte, A.; Gremaud, R.; Cerenius, Y.; Dornheim, M.; Klassen, T.; Bormann, R. J. Phys. Chem. C **2008**, 112, 2743-2749.

(16) Wang, X.L.; Hagiwara, H.; Suda, S. Vacuum **1996**, 47, 899-902.

(17) Brinks, H.W.; Fostal, A.; Hauback, B.C. J. Phys. Chem. C **2008**, 112, 5658-5661.

(18) Eigen, N.; Boesenberg, U.; Bellosta von Colbe, J.; Jensen, T.R.; Cerenius, Y.; Dornheim, M.; Klassen, T.; Bormann, R. J. Alloys and Compounds **2009**, 477, 76-80.

(19) Suarez-Alcantara, K.; Boesenberg, U.; Zavorotynska, O.; Bellosta von Colbe, J.; Taube, K.; Baricco, M.; Klassen, T.; Dornheim, M. J. Solid State Chem. **2011**, 184, 3104–3109.

(20) Stern, E.A. *Theory of EXAFS, in: D.C. Koningsberger, R. Prins, X-Ray absorption. Principles, Applications, Techniques of EXAFS, SAXAFS and XANES*; John Wiley & Sons, New York, 1988.

(21) Cerenius, Y.; Stahl, K.; Svensson, L.A.; Ursby, T.; Oskarsson, A.; Albertsson, J.; Liljas, A. J. Synchrotron Rad. **2000**, 7, 203-208.

(22) Ronnebro, E.; Majzoub, E.H. J. Phys. Chem. B **2007**, 111, 12045-12047.

(23) Riktor, M.D.; Sorby, M.H.; Chlopek, K.; Fichtner, M.; Hauback B.C. J. Mater. Chem. **2009**, 19, 2754-2759.

(24) Filinchuk, Y.; Ronnebro, E.; Chandra, D. Acta Materialia **2009**, 57, 732-738.

(25) Buchter, F.; Lodziana, Z.; Remhof, A.; Friedrichs, O.; Borgschulte, A.; Mauron, P.; Zuttel, A.; Sheptyakov, D.; Barkhordarian, G.; Bormann, R.; Chlopek, K.; Fichtner, M.; Sorby, M.; Riktor, M.; Hauback, B.; Orimo, S. J. Phys. Chem. B **2008**, 112, 8042-8048.

(26) Buchter, F.; Lodziana, Z.; Remhof, A.; Friedrichs, O.; Borgschulte, A.; Mauron, P.; Zuttel, A.; Sheptyakov, D.; Chlopek, K.; Fichtner, M.; Barkhordarian, G.; Bormann, R.; Hauback, B.C. J. Phys. Chem. C **2009**, 113, 17223-17230.

(27) Riktor, M.D.; Sorby, M.H.; Chlopek, K.; Fichtner, M.; Buchter, F.; Zuttel, A.; Hauback, B.C. J. Mater. Chem. **2007**, 17, 4939-4942.

(28) Gosalawit-Utke, R.; Suarez, K.; Bellosta von Colbe, J.M.; Bösenberg, U.; Jensen, T.R.; Cerenius, Y.; Bonatto Minella, C.; Pistidda, C.; Barkhordarian, G.; Schulze, M.; Klassen, T.; Bormann, R.; Dornheim, M. J. Phys. Chem. C **2011**, 115, 3762-3768.

(29) Rongeat, C.; D'anna, V.; Hagemann, H.; Borgschulte, A.; Zuttel, A.; Schultz, L.; Gutfleisch, O. J. Alloys and Compounds **2010**, 493, 281-287.

(30) Kim, J.H.; Shim, J.H.; Cho, Y.W. J. of Power Sources **2008**, 181, 140-143.

(31) Lee, J.Y.; Lee, Y.S.; Suh, J.Y.; Shim, J.H.; Whan, C.Y. J. of Alloys and Compounds **2010**, 506, 721-727.

(32) Brice, J.F.; Courtois, A.; Aubry, J. J. Sol. State Chem. **1978**, 24, 381-387.

(33) Lee, C.H.; Sohn, H.J.; Kim, M.G. Solid State Ionics **2005**, 176, 1237-1241.

(34) Jimenez, I.; Jankowski, A.F.; Terminello, L.J.; Sutherland, D.G.J.; Carlisle, J.A.; Doll, G.L.; Tong, W.M.; Shuh, D.K.; Himpsel, F.J. Physical Review B **1997**, 55, 12025-12037.

(35) Jimenez, I.; Sutherland, D.G.J.; van Buuren, T.; Carlisle, J.A.; Terminello, L.J.; Himpsel, F.J. Physical Review **1998**, 57, 13167-13174.

(36) Handa, H.; Kojima, K.; Taniguchi, K.; Ozutsumi, K.; Ikeda, S. Memories Sr. Center Ritsumeikan Univ. **2005**, 7, 3.

(37) Hayakawa, S.; Hajima, Y.; Qiao, S.; Namatame, H.; Hirokawa, T. Analytical Sciences **2008**, 24, 835-837.

(38) Galas, G.; Petiau, J. Solid State Communications **1983**, 48, 625-629.

Figure caption

Graphical abstract. In situ SR-PXD patterns of as milled $3CaH_2+4MgB_2+CaF_2$ composite, hydrogenation at 130 bar of H_2 and heating from room temperature to 350°C, lateral view (5 °C min^{-1}, λ=0.939Å, Max Lab Synchrotron).

Fig. 1. In situ SR-PXD patterns of as milled $3CaH_2+4MgB_2+CaF_2$ composite, hydrogenation at 130 bar of H_2 and heating from room temperature to 350°C, map view (5 °C min^{-1}, λ=0.939Å, Max Lab Synchrotron).

Fig. 2. In situ SR-PXD patterns of first dehydrogenation of $3CaH_2+4MgB_2+CaF_2$ (pre-hydrogenated) composite, dehydrogenation at 0.1 bar H_2 and heating from room temperature to 350°C (5 °C min^{-1}, λ=0.939Å, Max Lab Synchrotron).

Fig. 3. In situ SR-PXD patterns of second dehydrogenation of $3CaH_2+4MgB_2+CaF_2$ composite, dehydrogenation at 0.1bar H_2 and heating from room temperature to 350°C (5 °C min^{-1}, λ=0.7Å, ESRF Synchrotron).

Fig. 4. B K-edge spectra of $Ca(BH_4)_2+MgH_2$ and $Ca(BH_4)_2+CaF_2$ as milled. Inset: B K-edge spectra of un-milled $Ca(BH_4)_2$, $Ca(BF_4)_2$ and MgB_2 (Antares beamline, Soleil Synchrotron).

Fig. 5. B K-edge spectra of $3CaH_2+4MgB_2+CaF_2$ composite in hydrogenated (ab) and dehydrogenated (de) stages. $Ca(BF_4)_2$ and $Ca(BH_4)_2+CaF_2$ as reference materials (Antares beamline, Soleil Synchrotron).

Fig. 6. XANES Ca K-edge spectra of CaH_2, CaF_2, $Ca(BH_4)_2$, $Ca(BF_4)_2$ and $3CaH_2+4MgB_2+CaF_2$ after the 1st hydrogenation (A1 beamline, DESY synchrotron).

Fig. 7. Fourier transform of the XANES signals at the Ca K-edge of CaF_2, CaH_2, $Ca(BH_4)_2$ and $3CaH_2+4MgB_2+CaF_2$ after the 1st hydrogenation (1 ab), after the 1st dehydrogenation, (1 des) and after the 2nd hydrogenation (2 ab) (XAFS2 beamline, LNLS synchrotron).

Figures

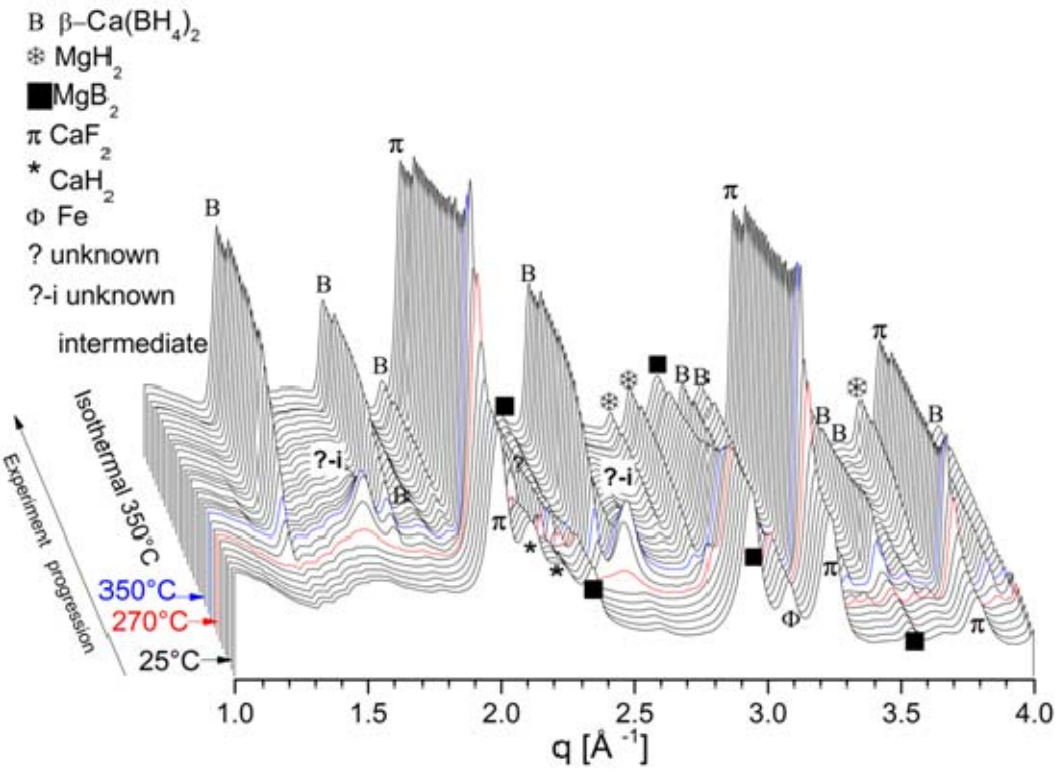

Graphical abstract. In situ SR-PXD patterns of as milled $3CaH_2+4MgB_2+CaF_2$ composite, hydrogenation at 130 bar of H_2 and heating from room temperature to 350°C, lateral view (5 °C min^{-1}, λ=0.939Å, Max Lab Synchrotron).

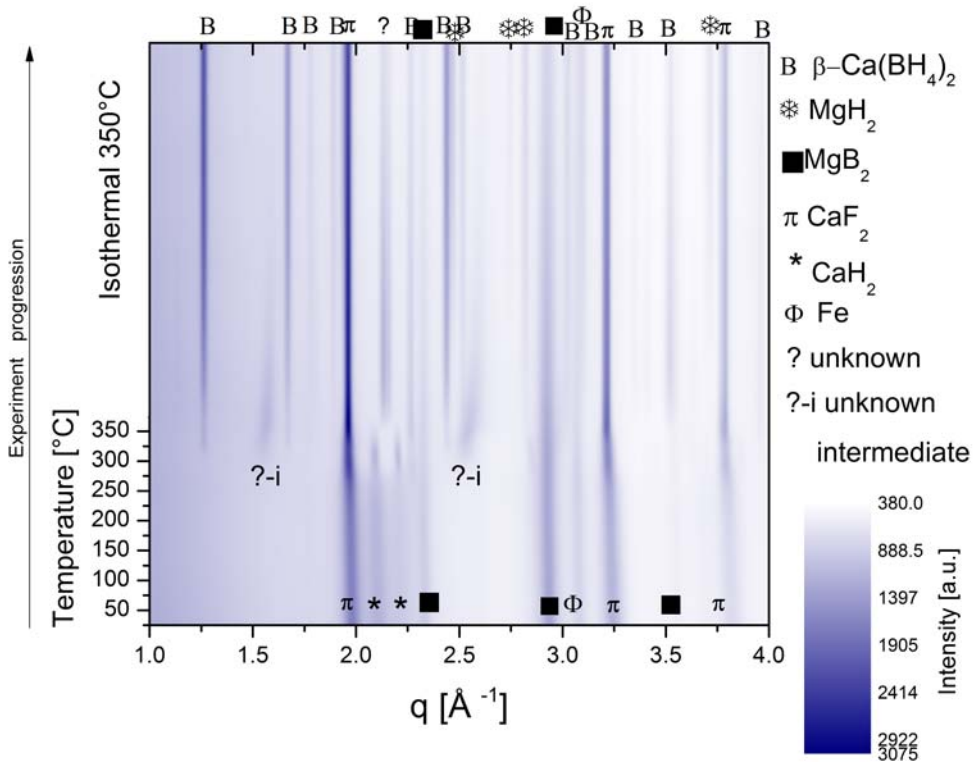

Fig. 1. In situ SR-PXD patterns of as milled $3CaH_2+4MgB_2+CaF_2$ composite, hydrogenation at 130 bar of H_2 and heating from room temperature to 350°C, map view (5 °C min^{-1}, λ=0.939Å, Max Lab Synchrotron).

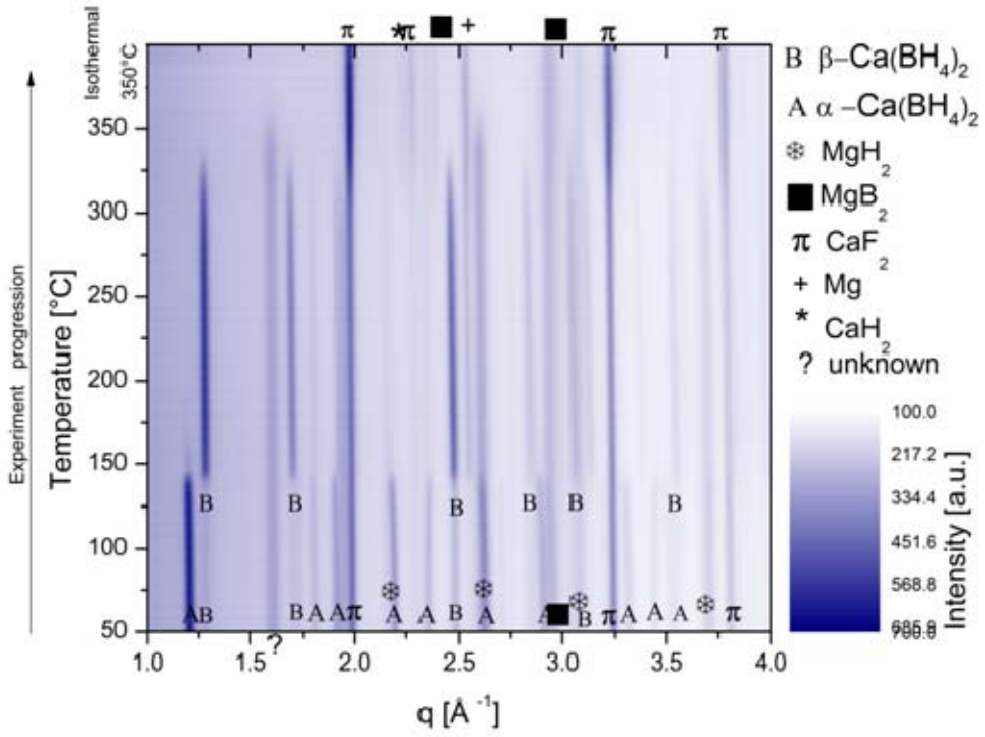

Fig. 2. In situ SR-PXD patterns of first dehydrogenation of $3CaH_2+4MgB_2+CaF_2$ (pre-hydrogenated) composite, dehydrogenation at 0.1 bar H_2 and heating from room temperature to 350°C (5 °C min^{-1}, λ=0.939Å, Max Lab Synchrotron).

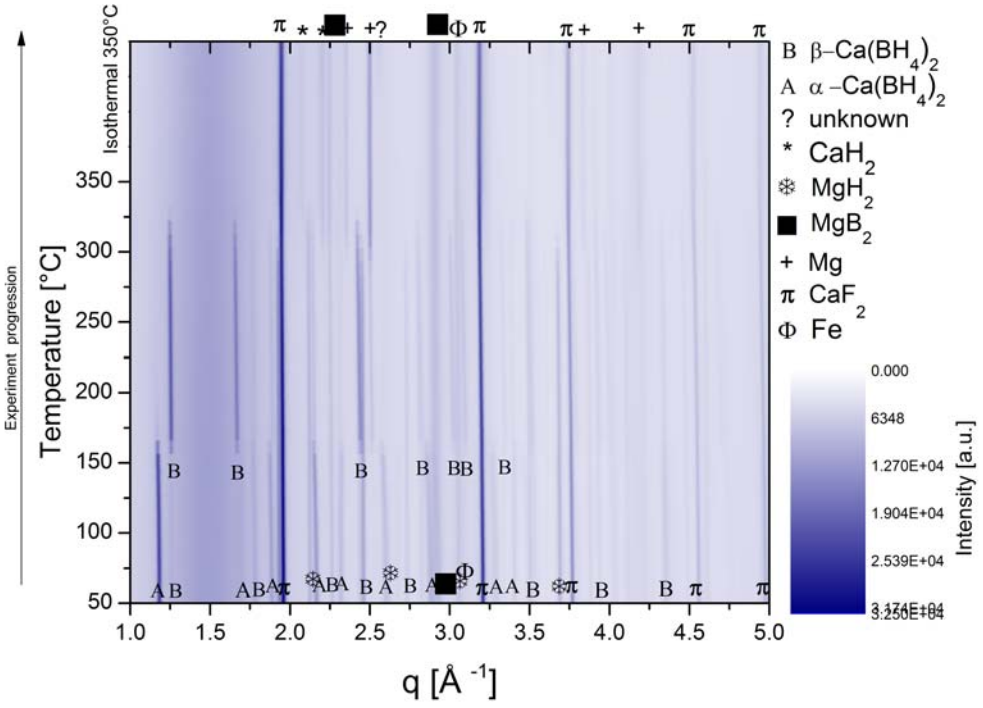

Fig. 3. In situ SR-PXD patterns of second dehydrogenation of $3CaH_2+4MgB_2+CaF_2$ composite, dehydrogenation at 0.1bar H_2 and heating from room temperature to 350°C (5 °C min^{-1}, λ=0.7Å, ESRF Synchrotron).

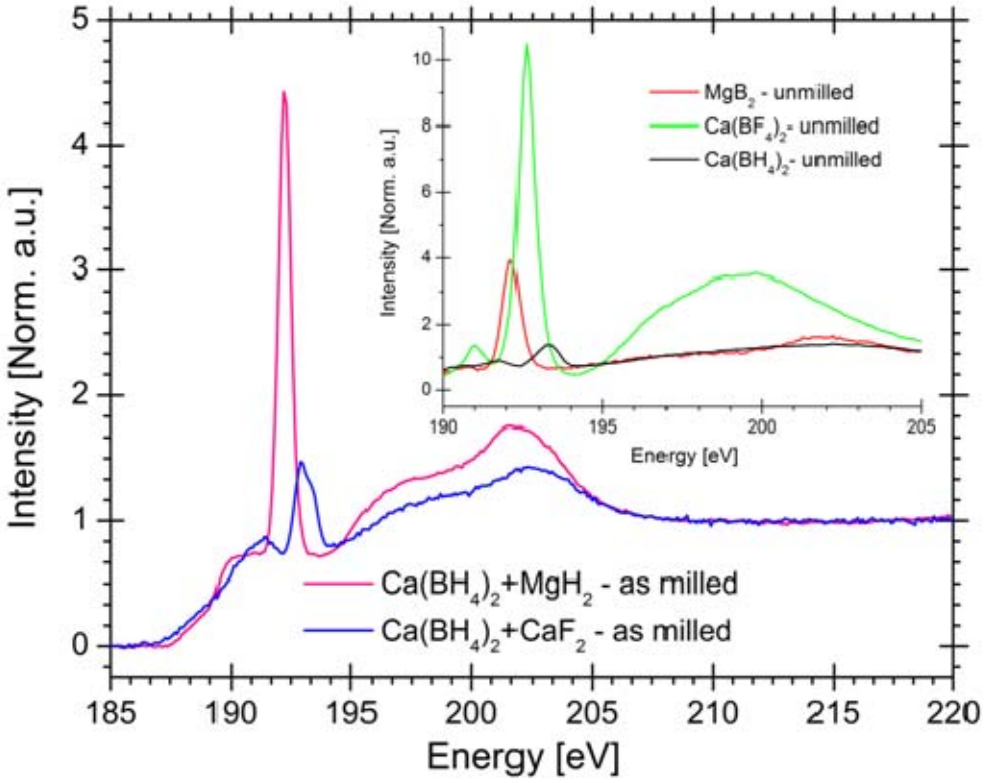

Fig. 4. B K-edge spectra of $Ca(BH_4)_2$+MgH_2 and $Ca(BH_4)_2$+CaF_2 as milled. Inset: B K-edge spectra of un-milled $Ca(BH_4)_2$, $Ca(BF_4)_2$ and MgB_2 (Antares beamline, Soleil Synchrotron).

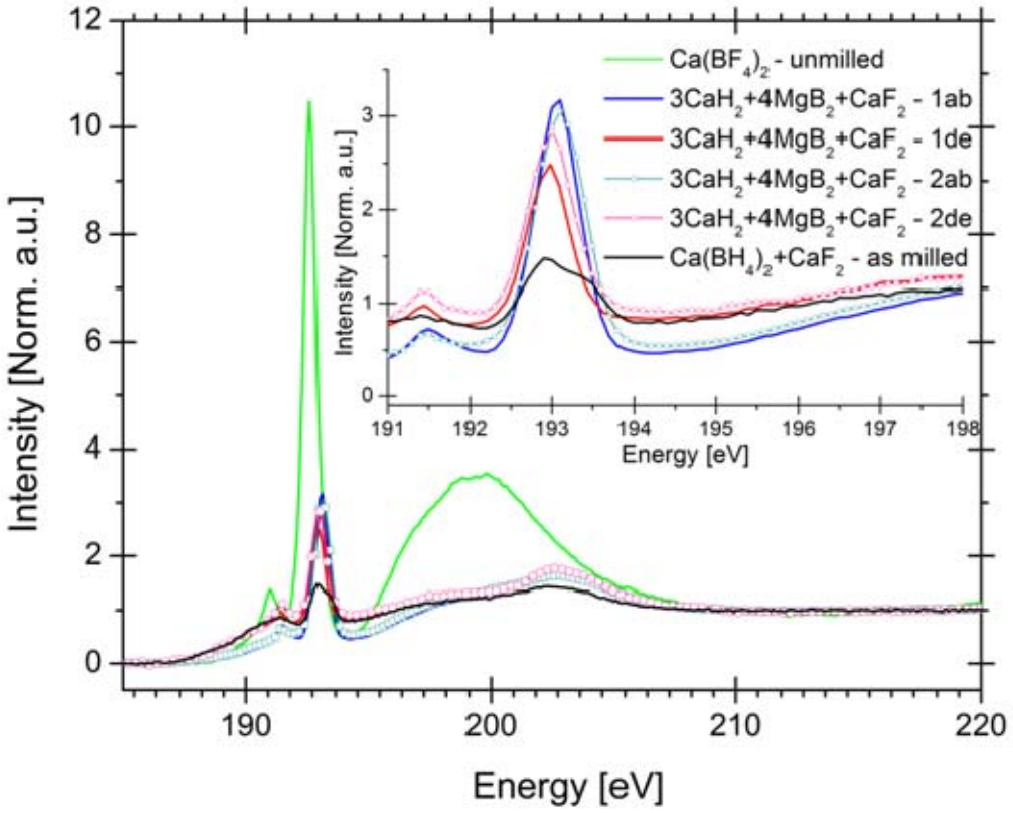

Fig. 5. B K-edge spectra of $3CaH_2+4MgB_2+CaF_2$ composite in hydrogenated (ab) and dehydrogenated (de) stages. $Ca(BF_4)_2$ and $Ca(BH_4)_2+CaF_2$ as reference materials (Antares beamline, Soleil Synchrotron).

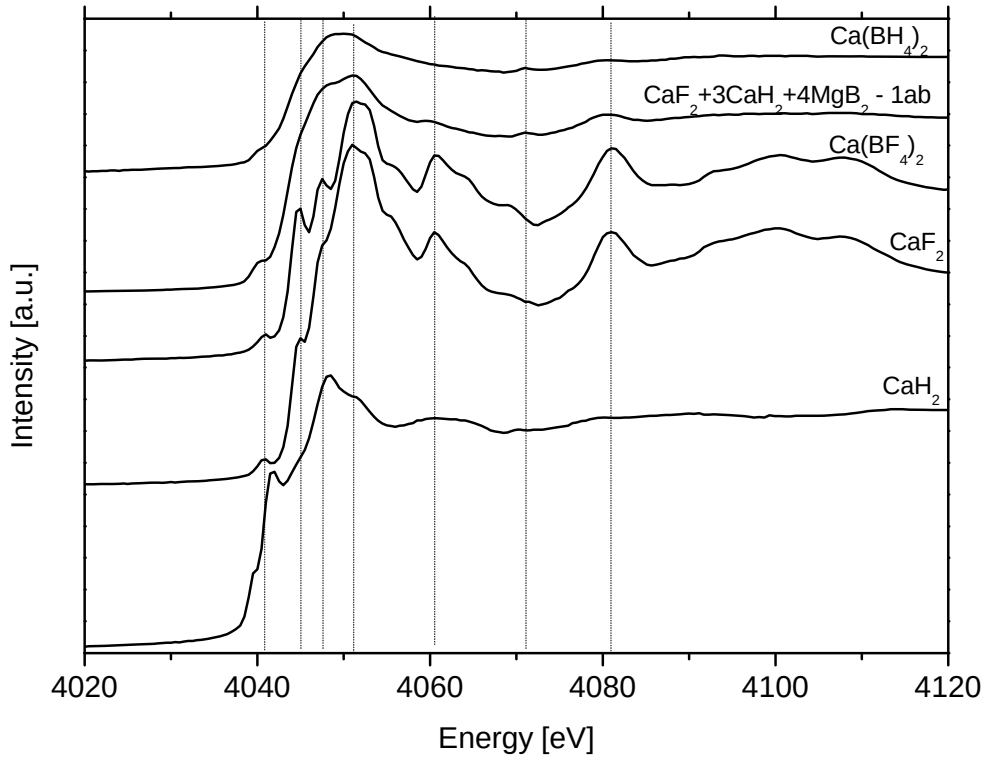

Fig. 6. XANES Ca K-edge spectra of CaH_2, CaF_2, $Ca(BH_4)_2$, $Ca(BF_4)_2$ and $3CaH_2+4MgB_2+CaF_2$ after the 1st hydrogenation (A1 beamline, DESY synchrotron).

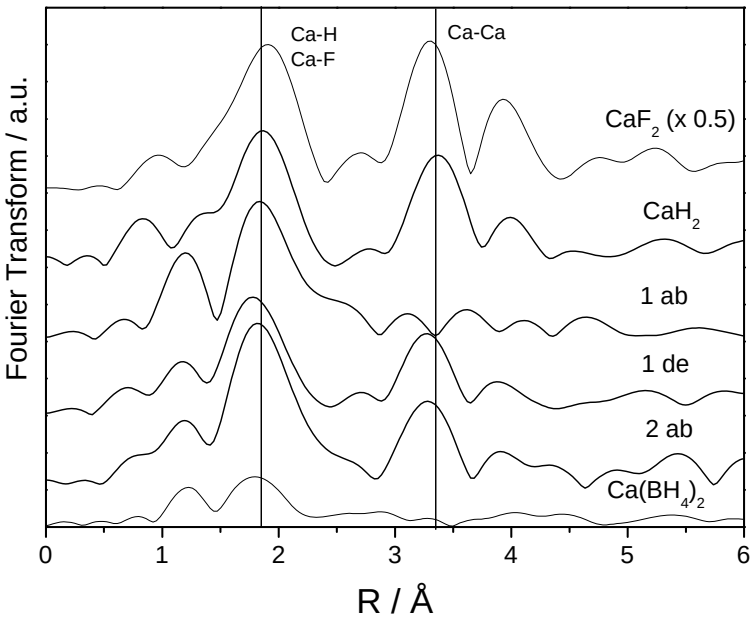

Fig. 7. Fourier transform of the XANES signals at the Ca K-edge of CaF_2, CaH_2, $Ca(BH_4)_2$ and $3CaH_2+4MgB_2+CaF_2$ after the 1st hydrogenation (1 ab), after the 1st dehydrogenation, (1 des) and after the 2nd hydrogenation (2 ab) (XAFS2 beamline, LNLS synchrotron).